remote sensing

MDPI

Article

Enhancing Underwater LiDAR Accuracy Through a Multi-Scattering Model for Pulsed Laser Echoes

Ruichun Dong [1], Xin Fang [1,2,*], Xiangqian Meng [3], Chengyun Yang [1,2] and Tao Li [1,2]

[1] CAS Key Laboratory of Geospace Environment, School of Earth and Space Sciences, University of Science and Technology of China, Hefei 230026, China
[2] CAS Center for Excellence in Comparative Planetology, University of Science and Technology of China, Hefei 230026, China
[3] College of Ocean Science and Engineering, Shandong University of Science and Technology, Qingdao 266590, China
* Correspondence: xinf@ustc.edu.cn

Abstract

In airborne LiDAR measurements of shallow water bathymetry, conventional data processing often overlooks the radiative losses associated with multiple scattering events, affecting detection accuracy. This study presents a Monte Carlo-based approach to construct a mathematical model that accurately characterizes the multiple returns in airborne laser bathymetric systems. The model enables rapid simulation of laser propagation through water, accounting for multiple scattering events. Based on the Beer–Lambert law and incorporating the parameters of typical Jerlov 1 clear coastal water, the proposed model achieves a seamless integration of the H-G phase function with a Monte Carlo random process, enabling accurate simulation and validation of pulse temporal broadening in waters with varying optical transparency. Unlike most existing studies, which primarily focus on modeling the laser emission process, this work introduces a novel perspective by analyzing the probability of light reception in LiDAR return signals, offering a more comprehensive understanding of signal attenuation and detection performance in underwater environments. The results demonstrate that, for detecting underwater targets at depths of 10 m, considering three or more scattering events improves the accuracy by ~7%. For detecting underwater targets at depths of 50 m, considering three or more scattering events improves the accuracy by 15~33%. These findings can help enhance the detection accuracy and efficiency of experimental systems.

Keywords: marine LiDAR; ALB system; Monte Carlo method; pulse temporal broadening; echo optical reception

Academic Editors: Alfonso Farina, Silvia Liberata Ullo, Yu Yao, Harun Taha Hayvaci and Pia Addabbo

Received: 18 April 2025
Revised: 27 June 2025
Accepted: 29 June 2025
Published: 30 June 2025

Citation: Dong, R.; Fang, X.; Meng, X.; Yang, C.; Li, T. Enhancing Underwater LiDAR Accuracy Through a Multi-Scattering Model for Pulsed Laser Echoes. *Remote Sens.* **2025**, *17*, 2251. https://doi.org/10.3390/rs17132251

1. Introduction

Shallow water areas around coasts and islands are critical regions that affect maritime navigation safety. Many countries have had to gain significant safety insights from events resulting from the lack of accurate knowledge of seabed topography. Reliable and high-resolution mapping of these shallow-water zones remains an urgent technical challenge critical to maritime safety. Our team has developed a prototype airborne LiDAR bathymetry system for comprehensive and high-precision topographic surveys of intertidal zones, mudflats, and reefs in shallow water areas. Equipped with an active pulse LiDAR system, the UAV can rapidly scan coastlines on both sides, covering a distance of nearly 100 km [1]. The principle of active pulsed LiDAR detection mounted on an unmanned aerial vehicle

(UAV) is illustrated in Figure 1. As shown in Figure 1, the laser beam emitted by the airborne LiDAR system is partially reflected and refracted upon contact with the water surface, and then propagates through the water column and reaches the seafloor. There, it interacts with various scatterers within the bottom sediments, causing part of the laser energy to be scattered at different angles and return to the LiDAR receiver. This process enables the acquisition of full-waveform data that captures the entire light–matter interaction along the transmission path [2].

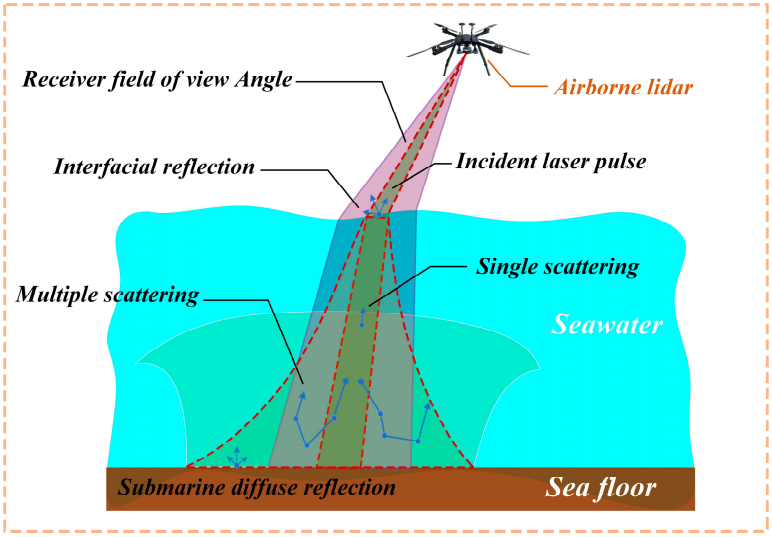

Figure 1. Schematic of airborne LiDAR detection.

The waveform signal received by the airborne bathymetric LiDAR system depends on the transmission waveform of the laser pulse, the spatial energy distribution of the beam, and the geometric characteristics and reflectivity of the target surface. The received full-waveform data clearly reveal two distinct echo peaks corresponding to the sea surface and the seafloor. The target depth can be calculated by measuring the time difference between these two reflected signals [3]. However, the accuracy of the measurement is influenced by factors such as seawater properties, environmental conditions, and flight altitude. Underwater laser transmission involves multiple scattering processes. Preisendorfer [4] was one of the earliest researchers to propose ocean optics theories, which many researchers have since expanded to include radiation transfer theories suitable for marine environments. Arnush [5] studied the theory of underwater light radiation transfer in Mie scattering environments and derived analytical solutions for underwater transmitted light fields. Lutomirski [6] solved the radiation transfer equation using Green's function and established a relationship between the beam transmission depth and the spatial distribution of radiation. Although these methods provide precise calculations, the solutions often incur substantial computational costs. Moreover, the theoretical models employed in conventional analytical methods significantly simplify the seawater characteristics during computation, leading to considerable deviations from real-world scenarios [7,8].

Conventional analytical methods are challenging to apply in engineering designs, and platforms for marine LiDAR (aircraft, UAVs, and satellites) make large-scale experiments prohibitively expensive. The Monte Carlo method offers a feasible shortcut to solving these challenges [9,10], enabling rapid and accurate simulation of laser transmission in random media. Bucher [11,12] introduced a Monte Carlo method to study multiple scattering processes of photons in various media. Lerner and Wang [13] subsequently refined and updated photon transport models in media. Numerous practical results have confirmed that Monte Carlo methods produce outcomes that are highly consistent with experimental

methods. It has become a common tool for studying light transmission in random media because it can simulate various parameters' effects on seawater laser transmission [2].

Conventional data processing typically assumes a single scattering process, neglecting the radiative losses associated with multiple scattering, which can affect the detection accuracy of the current airborne laser bathymetric system prototype [14,15]. To address this issue, this study developed a Monte Carlo-based mathematical model to align with the multiple-echo characteristics of existing airborne laser bathymetry prototypes [16]. Additionally, while multiple scattering has been extensively studied in underwater optical communication and imaging, it remains largely unexplored in the context of airborne bathymetric LiDAR [17–19]. This study proposes an analysis of the light reception probability of LiDAR return signals, aiming to enhance the detection accuracy and measurement efficiency of the current active airborne laser bathymetric system.

2. Key Issues

2.1. Simulation and Analysis of Multiple Scattering Characteristics in Underwater Laser Transmission

The light transmission window in seawater varies slightly between shallow and deep waters. In shallow areas, the transmissive wavelength range is 520~550 nm (optimal wavelength of 540 nm), while in deep waters, the transmissive range is 450~520 nm (optimal wavelength of 457 nm) [20]. Due to the maturity of research on 532 nm lasers in the blue-green spectrum and their advantages of small size, light weight, and high power, the 532 nm laser is the preferred choice for underwater detection. The airborne laser bathymetry system consists of several key functional units, including optical transmission and reception, data acquisition and control circuits, scanning mirrors, a global positioning system (GPS)–inertial measurement unit (IMU) integrated inertial navigation system, and data processing software. The prototype of the current airborne laser bathymetry system, along with its system composition and operational principles, is shown in Figure 2. The primary system parameters are listed in Table 1.

Table 1. Parameters of the airborne LiDAR bathymetric system.

System Parameters	Characteristic
Laser wavelength	532 nm
Laser repetition rate	5 kHz
Pulse width	1200 ps
Receiving field Angle	1 mrad
Laser spot radius	1.5 cm
Horizontal Position accuracy	0.01 m
Elevation measurement accuracy	0.05 m
Pitch and roll angle measurement accuracy	0.01°
Heading angle measurement accuracy	0.05°
Horizontal positioning accuracy	<0.01 m
Accuracy of elevation measurement	<0.02 m
Sounding range	Clean Water 0.7 $\sim$ 50 m
System power consumption	<200 W
Average Energy	35 μJ
Photons Emitted	1.23×10^{14}
Flight altitude	20 $\sim$ 100 m
Receiving telescope aperture	10 cm
Comprehensive sounding accuracy	0.2 m
Equipment weight	<20 kg

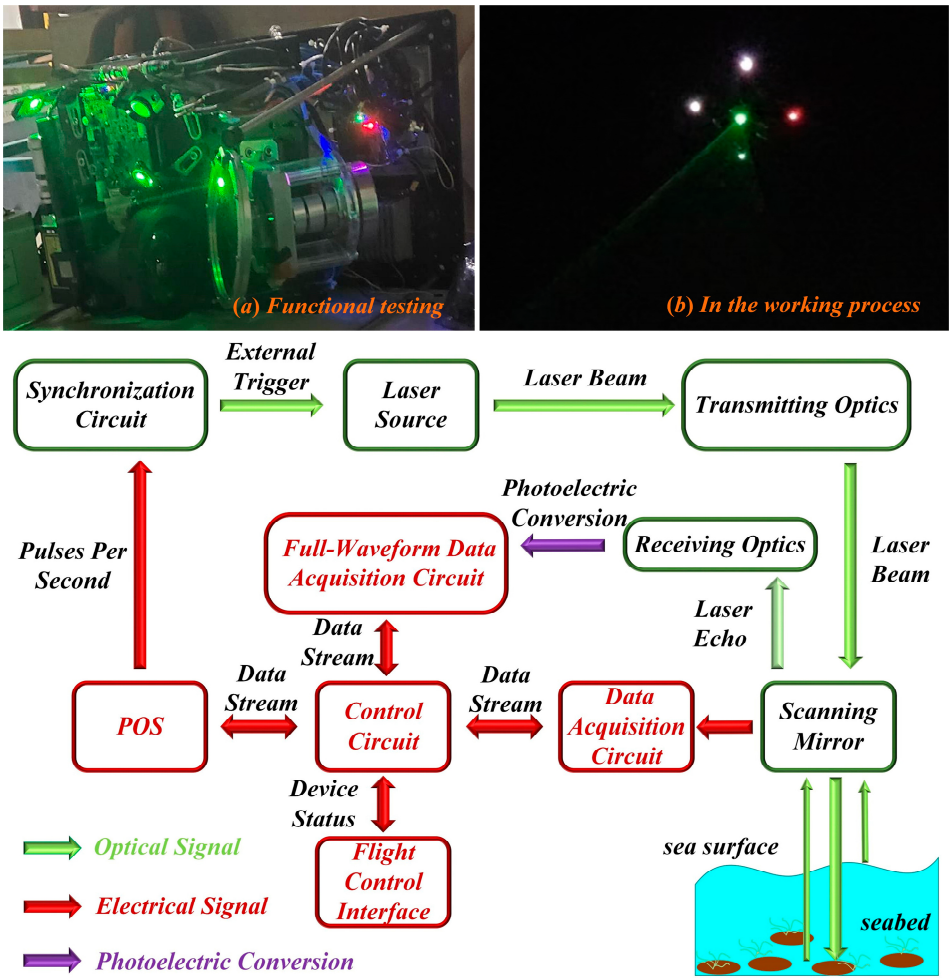

Figure 2. Prototype and system composition diagram of airborne LiDAR bathymetry system: (**a**) LiDAR equipment, structured and functional testing; (**b**) in the working process.

Based on the Beer–Lambert law and incorporating the parameters of typical Jerlov 1 clear coastal water [21], this study develops a model that captures the multiple scattering characteristics of the experimental system prototype. The model simulates the multiple scattering properties of laser light underwater from a photon perspective. A detailed explanation is provided below.

The computational power of standard computers is insufficient to simultaneously simulate the underwater transmission of hundreds of trillions of photons. The model was simplified to address this limitation and consider the characteristics of laser pulses by grouping all photons into photon packets for a unified motion analysis. The laser emits 5×10^3 pulses per second in the current experimental system, with each pulse recording data for 10^3 points. The number of photon packets was set to 5×10^6. Tracking the trajectories of millions of photon packets was deemed feasible in terms of both hardware capability and data reliability. An in-depth investigation of multiple scattering processes during the underwater transmission of pulsed lasers is essential for solving the radiative transfer problem [22]. The unsteady-state solution of the radiative transfer equation can be expressed as follows [23,24]:

$$\begin{aligned} &\tfrac{1}{v_{ph}} \tfrac{\partial}{\partial t} I(t,s,p) + n \nabla_s I(t,s,p) + c(t,s) I(t,s,p) \\ &= b(t,s) \int_{4\pi} I(t,s,p') \beta(t,s;p;p') dp' + Q(t,s,p) \end{aligned} \tag{1}$$

Here, v_{ph} is the speed of photon transmission in water, c and b are the beam attenuation coefficient and scattering coefficient, respectively, β is the scattering phase function and describes the probability of scattering from direction p to direction p', I is the irradiance, t is the transmission time, and s and p correspond to the position and direction vectors, $Q(t, s, p)$ describes the source of radiation at t, position s, and direction p. Based on the radiative transfer equation, seawater parameters, such as scattering and absorption coefficients, water quality, and laser transmission distance, were defined. A Monte Carlo stochastic model was employed to simulate the transmission process of the underwater lasers. The primary initial parameter settings of the model are listed in Table 2.

Table 2. Initial parameter settings of the Monte Carlo model.

System Parameters	Characteristic
Laser wavelength	532 nm
Initial photon energy weight	1
Asymmetry Factor of Seawater Medium	0.924
Number of simulated photon packets	5×10^6
Absorption coefficient of seawater	0.10 m^{-1}
Scattering coefficient of seawater	0.15 m^{-1}
Initial light source position	[0, 0, 0]
Refractive Index of seawater	1.33
Pulse repetition interval	1/5000 s
The Maximum scattering number of photons	0 $\sim$ 6
Laser underwater transmission distance	0 $\sim$ 50 m
Speed of laser light in seawater	3×10^8/1.33 m s^{-1}

This study proposes a Monte Carlo supervision algorithm that, based on a microscopic analysis model, captures the components of individual photons after scattering, reaching the detector's receiving plane at different depths. This allows the model to obtain a sufficient number of received signal samples. In the model, the laser beam is assumed to vertically incident downward from the sea surface, with seawater treated as a multilayer structure perpendicular to the beam's incident direction [25,26]. The Monte Carlo stochastic model, constructed based on the optical properties of the seawater medium, enables the precise and efficient simulation of LiDAR transmission signals. However, the model often requires significant computational resources to ensure the reliability of the simulation results [27–31].

As depicted in Figure 3, the key steps in implementing the Monte Carlo stochastic model can be succinctly summarized as follows: the photon position coordinates are initialized as $(x, y, z) = (0, 0, 0)$, and the directional cosines of motion are initialized as $(\mathrm{u}x, \mathrm{u}y, \mathrm{u}z) = (0, 0, -1)$. The laser incidence angle is determined by the initial cosine directional components $(\mathrm{u}x, \mathrm{u}y, \mathrm{u}z)$ of the motion vector. The photon energy weight is normalized to $W = 1$. Let the propagation direction of the photon after scattering be $\hat{\xi}'$, and the step length of the photon after the ith scattering be S_i; S_i can be determined using Bouguer–Lambert's law.

$$S_i = -\frac{1}{c} \ln \mathcal{R} \tag{2}$$

In Equation (2), the parameter c represents the total attenuation coefficient of the water body. The current position of the photon is iteratively updated based on its initial position coordinates and directional cosines of motion.

$$\begin{cases} x_{i+1} = x_i + ux_i \cdot S_i \\ y_{i+1} = y_i + uy_i \cdot S_i \\ z_{i+1} = z_i + uz_i \cdot S_i \end{cases} \tag{3}$$

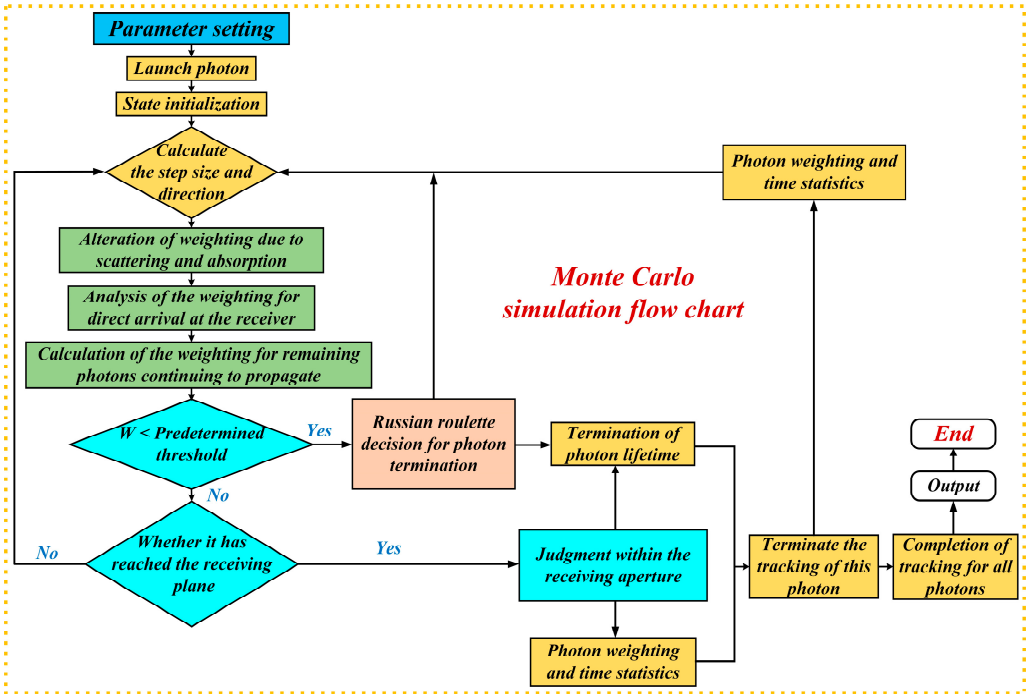

Figure 3. Flowchart of Monte Carlo simulation.

After each collision, the photons are evaluated randomly to determine whether they are absorbed or scattered. A random number $\mathcal{R}$ is selected from the interval $(0, 1)$ and compared with the albedo $W_0 = b/c$. The absorption of a photon is reflected in the change in its energy weight.

$$\mathrm{W} = \mathrm{W}\left(1 - \frac{a}{a+b}\right) = \mathrm{W}\left(\frac{b}{c}\right) = \mathrm{W}\,\mathrm{W}_0 \tag{4}$$

In Equation (4), $c = a + b$, where c is the total attenuation coefficient of the water body, a is the absorption coefficient, and b is the scattering coefficient. The photon's motion is continuously tracked until it is determined whether the photon was annihilated. After a collision, the change in the direction of motion is calculated by sampling the Henyey–Greenstein phase function to determine the azimuth angle φ and scattering angle θ.

$$\varphi = 2\pi\mathcal{R} \tag{5}$$

$$\theta = cos^{-1}\left(\frac{1+g^2-\left[\left(1-g^2\right)/(1-g+2g\mathcal{R})\right]^2}{2\mathrm{g}}\right) \tag{6}$$

In Equation (6), g is the asymmetry factor of seawater medium and $\mathcal{R}$ is a random number uniformly distributed in the interval [0, 1]. The final expressions for the directional cosines of motion can be derived by fixing at the *ith* collision point and combining the equations above.

$$\begin{cases} ux_{i+1} = \frac{sin\theta[ux_i \cdot uz_i \cdot cos\varphi - uy_i \cdot sin\varphi]}{\sqrt{1-uz_i^2}} + ux_i \cdot cos\theta \\ uy_{i+1} = \frac{sin\theta[uy_i \cdot uz_i \cdot cos\varphi - ux_i \cdot sin\varphi]}{\sqrt{1-uz_i^2}} + uy_i \cdot cos\theta \\ uz_{i+1} = -sin\theta \cdot cos\varphi\sqrt{1-uz_i^2} + uz_i \cdot cos\theta \end{cases} \tag{7}$$

Initially, only single-pass transmission is considered, with photon energy below the lower boundary set to zero, thus halting further migration. The model emphasizes the changes in photon energy resulting from interactions with suspended particles. An improved model is introduced by setting a death threshold, $W_{min} = 10^{-2}$, to terminate photon tracking when its weight falls below this threshold. It is possible to avoid processing many

low-weight photons without losing energy conservation. A Russian roulette mechanism is also incorporated [32]: if $W_{i+1} > W_{min}$, photon tracking continues; if $W_{i+1} < W_{min}$, a random number $\mathcal{R}'(0 < \mathcal{R}' < 1)$ is generated and compared with a preset probability threshold $PT(0 < PT < 1) = 0.2$. If $\mathcal{R}' < PT$, the photon continues to be tracked with a weight increase of PT; otherwise, the photon is considered to have "died" [33].

For the air/water interface, the change in photon weight and direction of motion can typically be calculated using Fresnel's reflection law [34]. However, due to the high frequency of the laser pulse, the time span of each pulse is extremely short, allowing the sea surface to be considered as stationary from a temporal perspective. Additionally, the full waveform data acquired by the LiDAR system clearly reveal distinct peak signals associated with reflections from the sea surface. After time integration, the distance from the radar to the sea surface can be precisely determined. Therefore, our study is confined to the region below the air/water interface, with the initial source position set at $[0,\ 0,\ 0]$.

Figure 4 shows the simulation results for the vertical laser incidence and normalized photon energy. As the number of scatterings increases during transmission, the laser beam becomes increasingly divergent, and the photon energy rapidly attenuates with depth. This attenuation follows the Beer–Lambert law [35]; considering both absorption and scattering, the laser intensity decreases exponentially with increasing transmission distance.

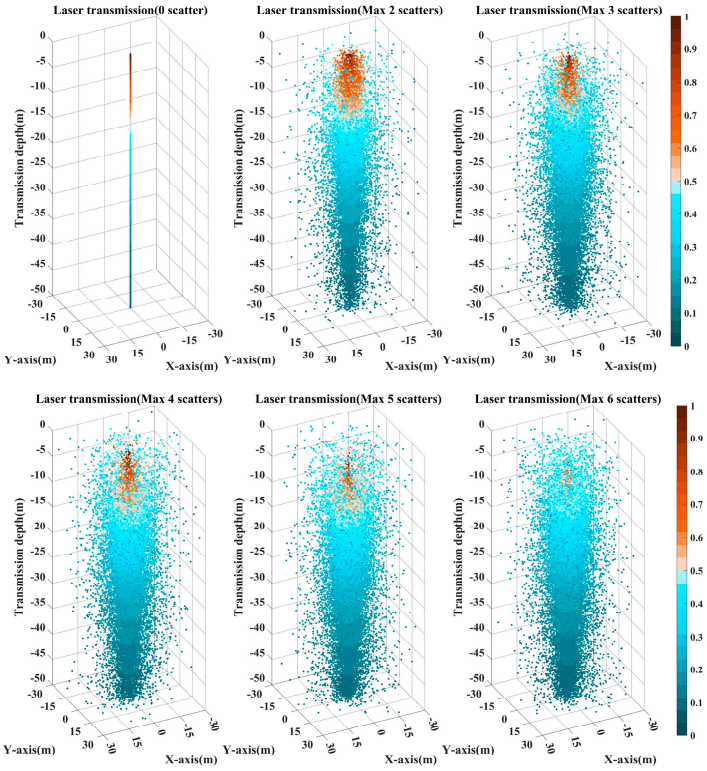

Figure 4. Simulation results after multi-scattering during the laser transmission process.

The statistical results for the number of photon packets received and their average energies at different depths are shown in Figure 5. It can be observed that as photons travel deeper, their energy weight decreases due to scattering and absorption, and the number of photon packets received by the detector decreases even more drastically than the reduction in energy weight. This indicates that a large number of photons are considered "died." Therefore, tracking only photons with higher weights is more efficient than tracking all photons, and this approach does not introduce significant errors in the results. This also validates the importance of setting the death threshold W_{min}.

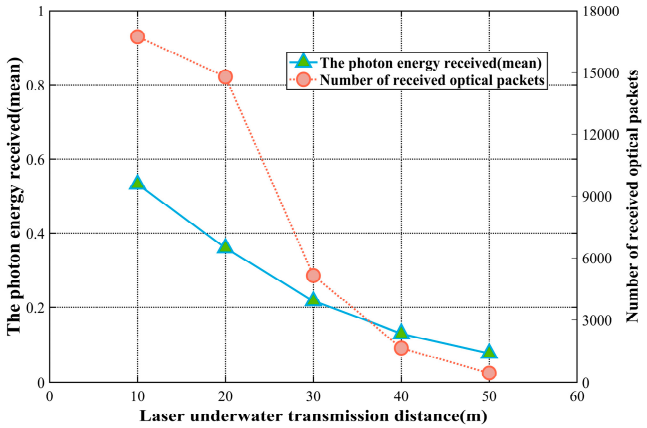

Figure 5. Number of photon packets received at different depths of the probe plane and their energy averages.

The scanning angle of the experimental system was fixed at 7.5°, resulting in a conical section with a cone angle of 15°. Vertical laser incidence is suitable for the qualitative analysis of underwater targets. However, changing the laser incidence angle for actual measurements is necessary. A comparative analysis was conducted for the typical incidence angles of 30°, 45°, and 60° with respect to the *z*-axis to examine the photon spatial distribution and energy variations at a depth of 10 m, as shown in Figure 6. To maintain consistent visual dimensions across images while accommodating the substantial variation in angle, we standardized the axis lengths and scale. However, we allowed the numerical ranges to vary to preserve detail and avoid obscuring key features.

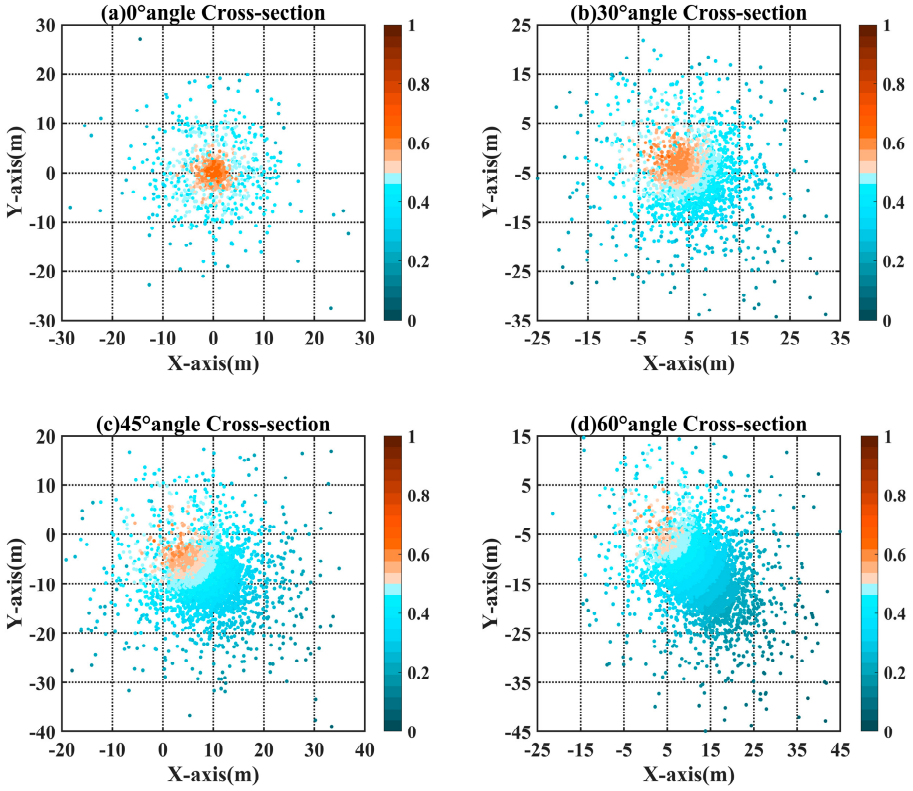

Figure 6. Spatial and energy variations of photons corresponding to different angles of laser incidence at 10 m underwater.

In Figure 6a–d, the photon energy shows a significantly banded, uneven distribution. In the case of conventional data processing, only a single scattering process of the laser

underwater is considered, not multiple scattering. A quantitative description of this issue is crucial for improving detection accuracy and reducing errors in airborne LiDAR systems. A quantitative analysis of the photon spatial and energy distributions at a depth of 10 m was conducted after the laser entered at different incidence angles. The probability density distribution of the photons in the x-direction within the receiving field of view was processed using a Gaussian function [32], as shown in Figure 7.

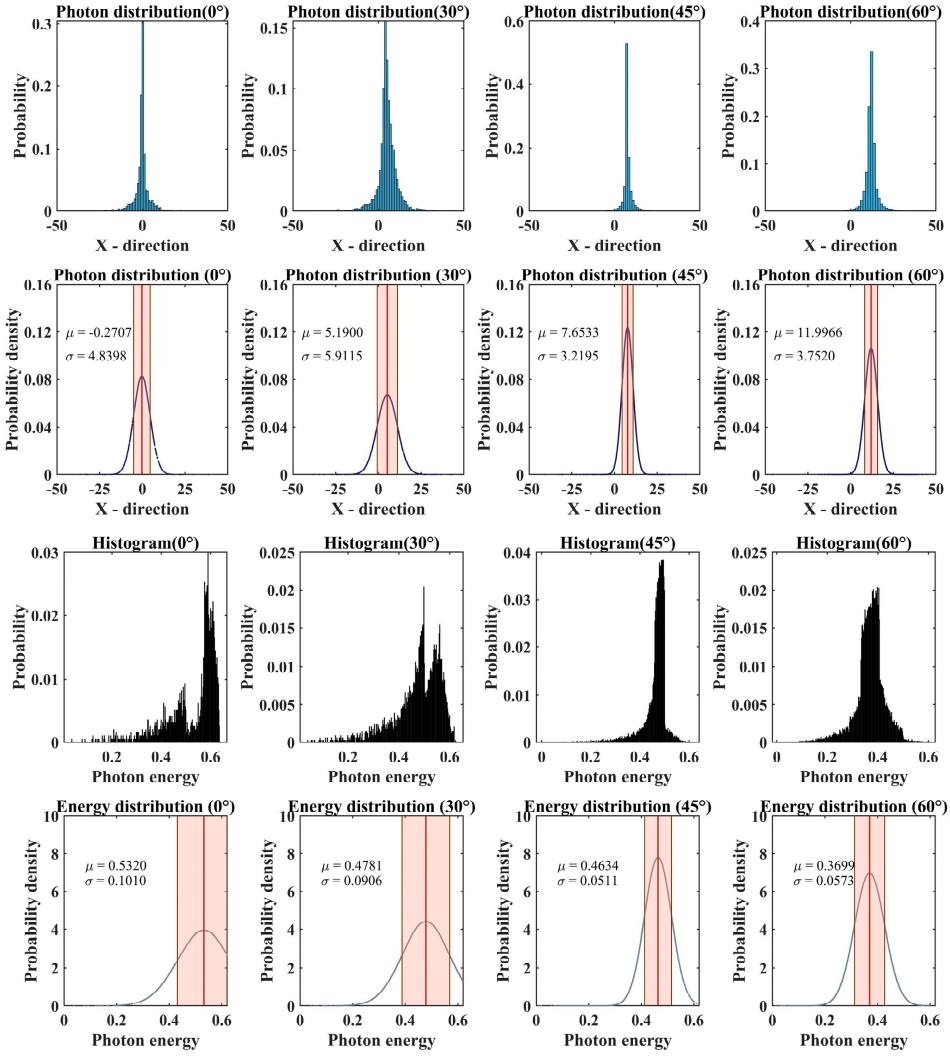

Figure 7. Spatial and energy distribution of photons received at the detection plane at a depth of 10 m in the x-direction.

The results presented in Figure 7 reveal several intriguing phenomena. The degree of waveform broadening of photons received at a depth of 10 m, following incidence at different angles, did not show a clear trend, indicating the irregular divergence of photons. When the incidence angle ranged from 0° to 30°, the photon distribution diverged. However, the photon distribution shifted toward convergence when the incidence angle increased from 30° to 45°. This phenomenon can be explained as follows: scattering predominates when the incidence angle is between 0° and 30°. In contrast, when it is between 30° and 45°, absorption, influenced by the geometric distance variations caused by the angle, becomes more dominant. Additionally, the irregular fluctuations in the peak can be attributed to the effective absorption of the photons scattered at the edges; this halts their migration and causes the Gaussian waveform to converge toward the center of the symmetry axis. We also observe that the small-angle energy distribution exhibits a bimodal pattern. This can be explained as follows: the smaller the angle, the shorter the path the

beam travels to reach a given depth. The high-energy peak indicates that the photons undergo fewer scattering events between emission and reception. As the incident angle increases, the path length increases, and the high-energy peak gradually shifts towards the low-energy peak, eventually merging into a single peak.

The classical lidar equation considers only a single backscattering event. In practice, however, particularly for underwater laser transmission, photons undergo multiple small-angle scatterings, deviating from straight-line propagation. This weakens the main beam, reduces the effective return signal, and degrades range resolution. Spatially, increased stray light and a lower proportion of target-return photons lead to image blurring and greater ranging errors. Given these conditions, a statistical analysis of photon scattering and energy variation is required. These effects can be mitigated by Monte Carlo simulations, which trace individual photon paths and their associated energy losses to enable more accurate modeling of scattering dynamics.

Figure 8 depicts the Gaussian distribution of the photon simulations for single scattering and three scattering events. Given a sufficiently large reception field of view, specifically one that encompasses the sea surface scanning range of the airborne sonar radar at an altitude of 50 m, the coverage area approximates an ellipse with a semi-major axis of 15 m; the error primarily stems from energy loss. By considering both the distribution of received photons and their energy characteristics at a depth of 10 m, the correction factor for errors caused by scattering can be derived as follows:

$$R_{total}(10) = R_{scatter}(10) \cdot R_{accept}(10) = \frac{\sigma_{discrete}(3)}{\sigma_{discrete}(1)} \cdot \frac{\mu_{energy}(1) - \mu_{energy}(3)}{\mu_{energy}(3)} \tag{8}$$

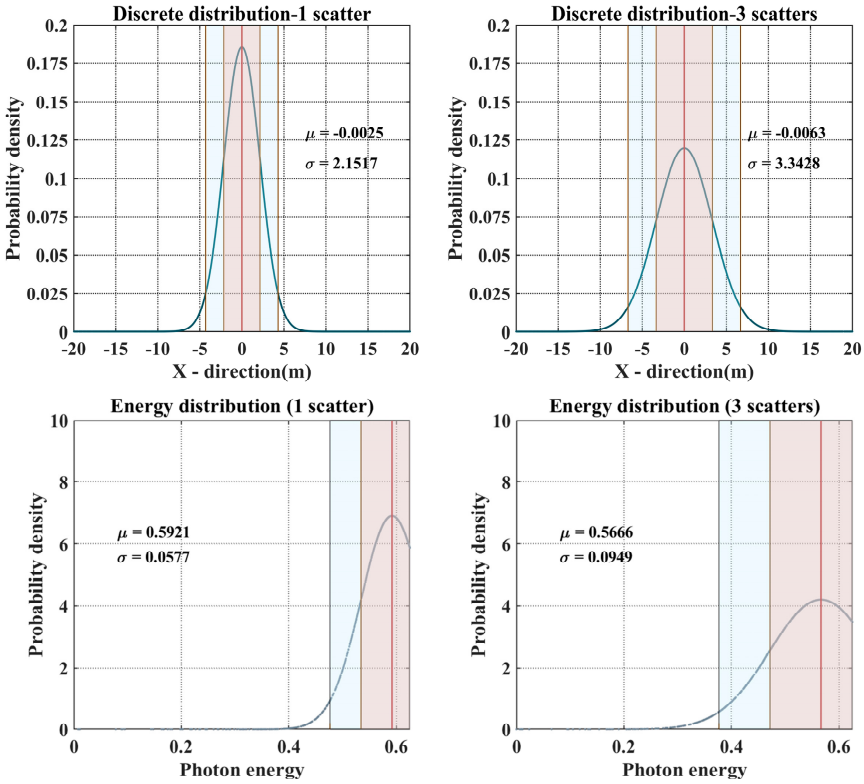

Figure 8. Simulation results of the model for single scattering and three scattering events of laser (at a depth of 10 m).

In Equation (8), R_{total} represents the total error correction factor, while $R_{scatter}$ refers to the scattering distribution error caused by different numbers of scattering events. This can be calculated as the ratio of the variance of the position distributions for three scattering

and single scattering events, $\sigma_{discrete}(3)/\sigma_{discrete}(1)$. R_{accept} represents the energy loss of photons, which directly affects the estimation of detection depth. This can be derived from the change in the mathematical expectation of the energy Gaussian distribution, $\left(\mu_{energy}(1) - \mu_{energy}(3)\right)/\mu_{energy}(3)$. Therefore, based on the results in Figure 8, it can be concluded that considering three scattering events, compared to considering only single scattering, can correct at least 6.992% of the error for detecting targets at a depth of 10 m. Considering the Monte Carlo error quantification, increasing the simulation runs and introducing a 95% confidence level, the error range is 6.992% $\pm$ 0.3%.

2.2. Simulation and Analysis of Temporal Broadening Characteristics of Laser Transmission Underwater

Interactions with suspended particles in seawater occur during the underwater transmission of a laser pulse. These interactions lead to two main effects: first, they cause the laser beam to diffuse during transmission, and second, multiple scattering results in multipath transmission, which causes temporal broadening of the laser pulse signal [35]. Since the H-G phase function is the preferred choice for simulating seawater scattering characteristics using the Monte Carlo method, this study combines it with Monte Carlo simulations to analyze the temporal broadening of laser pulse underwater transmission. An innovative approach is proposed by describing the temporal broadening of the waveform using the probability corresponding to the transmission time to the receiving plane. Compared to using amplitude as the vertical axis, this normalization method more effectively reflects the interactions occurring during laser underwater transmission. The factors influencing pulse broadening are then analyzed, starting with the impact of laser underwater transmission distance on pulse broadening.

At 40 cm and 50 cm underwater, detection planes were established while keeping the environmental parameters and other model conditions unchanged. The Monte Carlo random model simulation results for the pulse-broadening waveforms are shown in Figure 9a,b. A comparison of the two figures reveals that as the underwater laser transmission distance increased, the number of scattering events also increased, leading to a longer time from the start to the end of the pulse recording. The simulated waveform results closely match the actual detection scenarios, as shown in Figure 9c. Although the actual underwater transmission distances during testing were relatively short, a detailed analysis of the changes in a specific half-wave peak revealed that the magnitudes of broadening were comparable. It should be noted that individual pulses exhibit significant randomness. To improve reliability, Figure 9a,b show the temporal broadening based on the accumulation of 10 pulses. Figure 9c presents the pulse broadening observed during actual detection. Notably, to better resolve the characteristics of different seabed substrates, the experiment was conducted in relatively shallow water, resulting in a shorter laser propagation time. However, given the system's pulse repetition rate of 5×10^3 pulses per second, the integrated pulse signals yield time scales comparable to those observed in the simulation. In addition, the calculations indicate that the maximum effective temporal broadening is approximately five nanoseconds, corresponding to the longest optical path length. The simulation results and experimental results are of the same order of magnitude [16]. This consistency underscores the ability of the model to accurately simulate the temporal broadening characteristics observed in the practical experiments.

The asymmetry factor, g, characterizes the forward-scattering properties of seawater. The H-G phase function flexibly characterizes the angular distribution of scattering using the asymmetry parameter g. When $0 < g < 1$, forward scattering predominates, making it suitable for modeling typical particles in water. For airborne LiDAR bathymetry systems primarily utilized in shallow coastal waters with significant spatial variability in water quality, studying the influence of g on temporal pulse broadening is crucial for improving

the detection performance of current experimental prototypes as shown in Figure 10, using g = 0.924, which most closely matches Petzold's measured water quality parameters [36]. With deviations of ±0.025 and ±0.05, it is observed that larger asymmetry factors lead to reduced pulse broadening. The calculations indicate that increasing the asymmetry parameter g from 0.874 to 0.974 results in a 2.5-nanosecond decrease in temporal pulse broadening. This occurs because stronger forward scattering in seawater shortens the path length of scattered photons before they reach the detector's photosensitive surface, thereby minimizing temporal spread [36]. In the Monte Carlo random model, the seawater attenuation coefficient c governs the photon free path length, S. By maintaining consistent underwater environmental parameters and system conditions, simulations performed with c values of 0.25, 0.3, 0.35, and 0.4 demonstrated that an increase in the effective attenuation coefficient led to a more pronounced temporal broadening of the laser pulse. The calculations indicate that increasing the asymmetry parameter c from 0.25 to 0.4 results in a 3.5-nanosecond increase in temporal pulse broadening. This is because a larger attenuation coefficient shortens the average photon migration step length, increases the number of scattering events over the same transmission distance, and thereby results in more pronounced temporal broadening of the pulse. The model also demonstrates strong scalability, offering potential for future optimization of critical ALB system parameters, including scanning angle and pulse frequency, to improve detection performance and data fidelity.

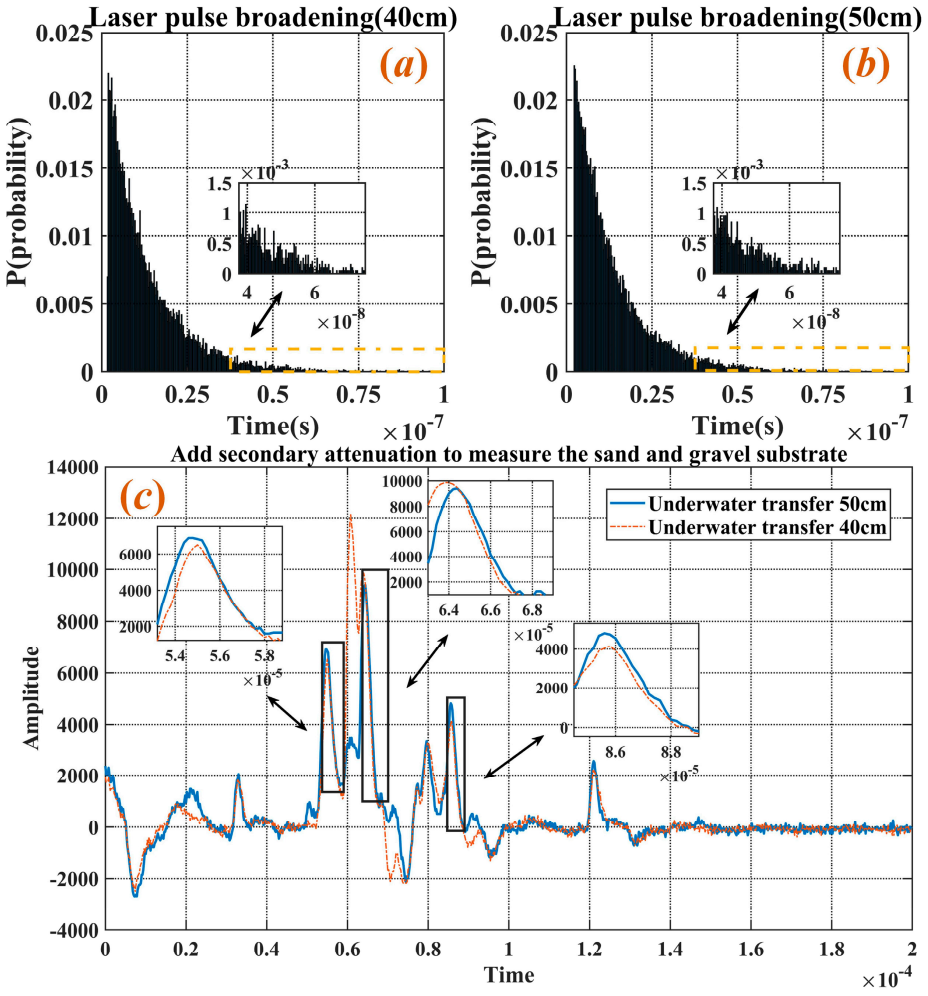

Figure 9. Comparison of pulse broadening at different laser transmission distances: (**a**) simulation results (40 cm); (**b**) simulation results (50 cm); (**c**) actual results.

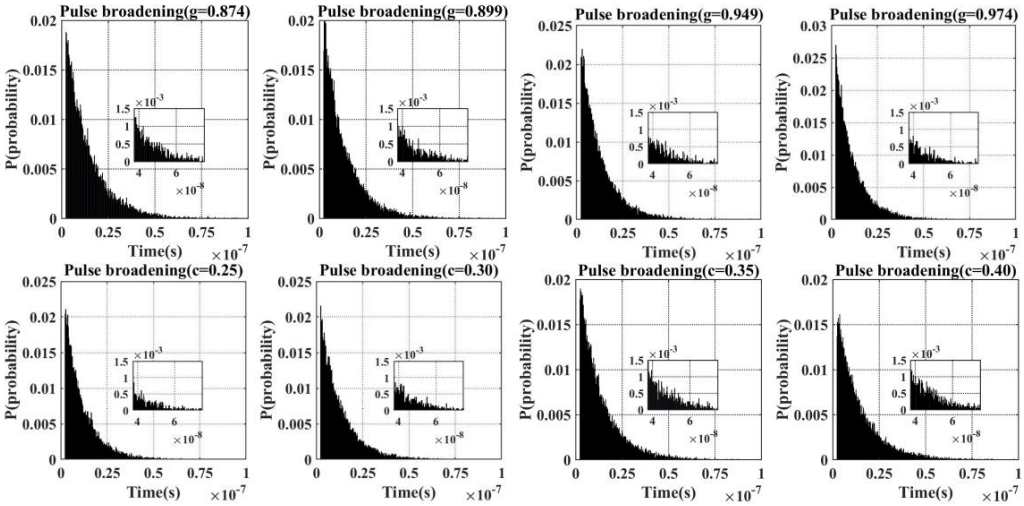

Figure 10. Comparison of laser pulse broadening with different values of g and c.

2.3. Simulation and Analysis of Airborne LiDAR Echo Light Reception Probability

To obtain underwater topographic information, an active airborne LiDAR bathymetry system requires receiving echo light and converting it into electrical signals after laser emission. However, most previous studies primarily focused on simulating the laser emission process using Monte Carlo methods, with little attention paid to modeling the echo light reception path in certain scenarios [37]. Therefore, simulating echo light reception probability using a Monte Carlo stochastic model is a novel research direction. By positioning the detection plane on the same level as the laser emission source, this study analyzed the probability of laser echoes returning to the receiving plane in an airborne LiDAR system.

The process of echo light reception, indicated by the green arrows in Figure 11a, involves the deflection of the laser light after interacting with a target at a certain depth. Based on the Monte Carlo random model, selecting the "seafloor" location, and placing a detector at the laser emission point to record photons that return to the sea surface. This introduces two main issues. First, the model predicts laser transmission from the perspective of photons, with the photon trajectory determined by randomly sampled directional cosines and migration step lengths. Determining whether a photon has reached the seafloor interface is challenging. The second issue is the design of the detection plane and filtering out non-seafloor echo lights. Solving these two problems is crucial for practically detecting the entire experimental system.

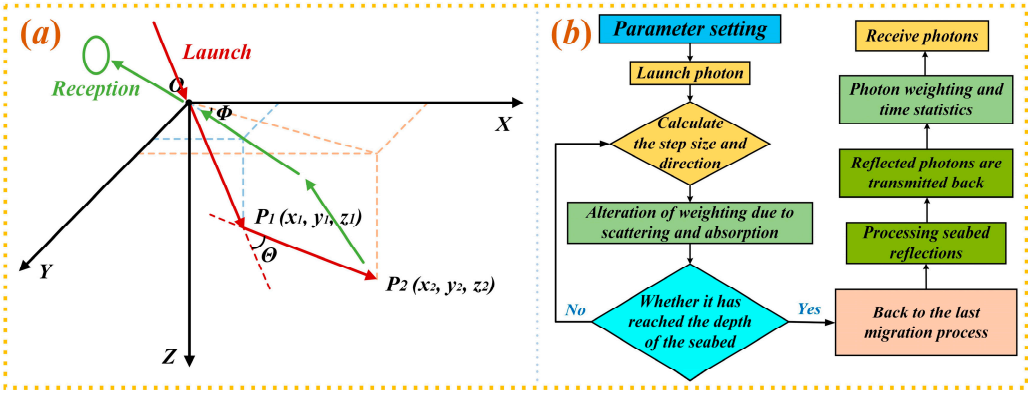

Figure 11. (**a**) Schematic of echo light reception in an airborne LiDAR bathymetric system; (**b**) flowchart of the modeling approach.

In response to these issues, the methods and modeling workflow illustrated in Figure 11b were implemented. The model assumes the seafloor is 50 m below the wa-

ter surface [38], with the seafloor being a Lambertian surface [39]. Upon reaching this depth, the incident light beam undergoes reflection. The inverse processing is applied to the Si step at which the light reaches the seafloor. The model identifies the photon's z-coordinate after the *ith* migration using seafloor depth as a threshold. If it exceeds the seafloor depth, the model traces back to the coordinates after the $(i-1)$th migration. If the value is below seafloor depth, the photon is considered to have crossed the seafloor during that step. The initial coordinates of this step are then retrieved using boundary processing at seafloor depth. The scattering and azimuth angles are also sampled, and the total laser emission time is recorded. The simulation results of the detector receiving the echo light are shown in Figure 12. Few photons returned to the sea surface and were detected by the receiver. It must be noted that the detector area provided in this study is sufficiently large.

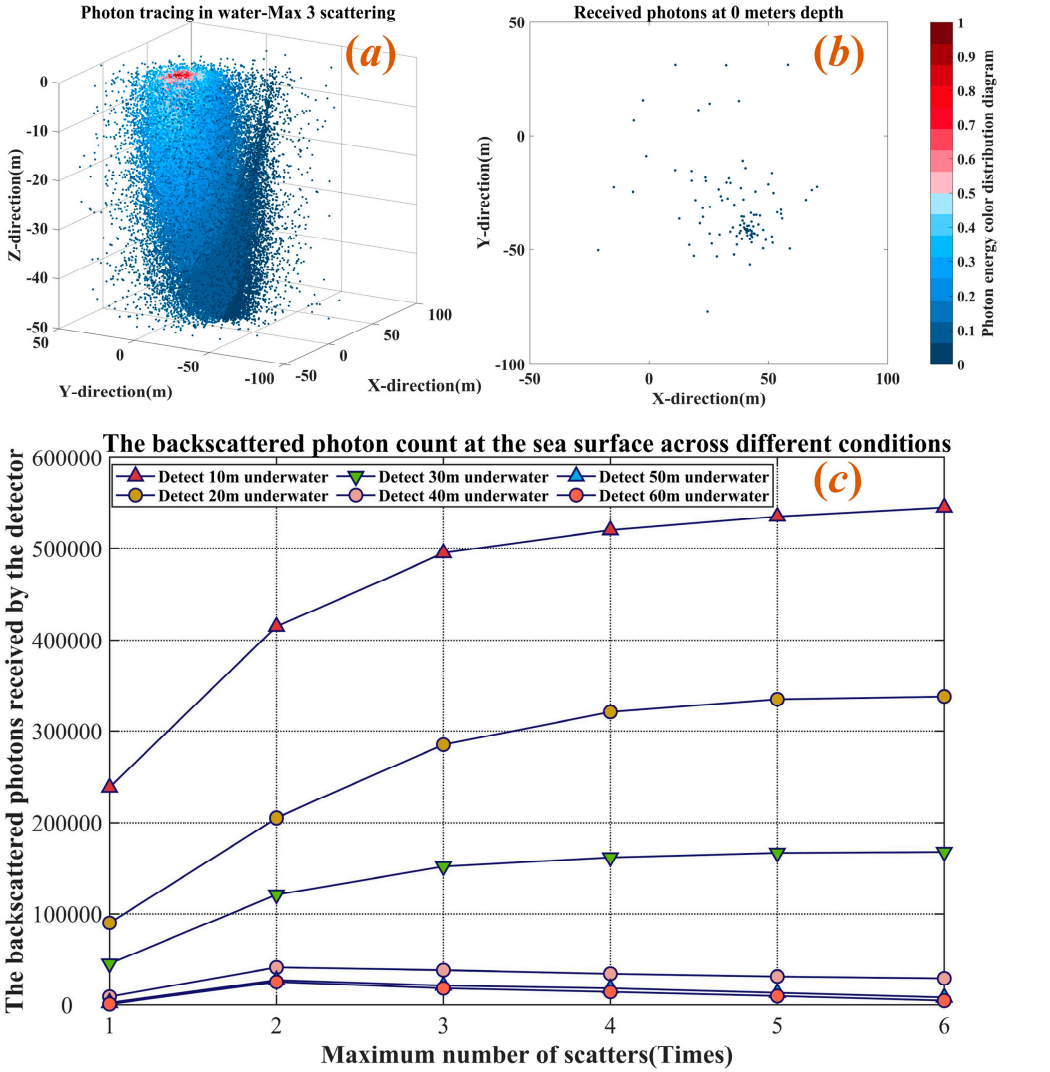

Figure 12. Number of photons received by the detector after laser transmission at different distances underwater: (**a**) photon tracing in water; (**b**) received photons at 0 m depth; (**c**) count of backscattered photons.

Although the actual number of photons may vary due to absorption or scattering, the normalized results presented in Figure 8 may obscure these changes, as all values are scaled to a uniform range. Therefore, it is essential to statistically track the number of photons received by the detector. The data in Figure 12 show that as the number of scatterings increased, the number of photons received by the detector at the sea surface followed a similar trend for the underwater transmission distances of 40, 50, and 60 m. However, at

a 10, 20, and 30 m transmission distance, the number of received photons and the overall trend changed significantly, which is intriguing. This can be attributed to the 30 m depth limit, which restricts the photons from completing their full trajectory. In other words, under the current mathematical model, the "scattering potential" of the photons is not thoroughly exhausted. When photons return to the receiving plane, their migration step lengths are determined. This indirectly confirms that the Monte Carlo random model is well suited for coastal waters shallower than 30 m. This aligns well with the operating domain of marine LiDAR, in which photons remain in a state always subject to scattering. This is closer to the actual measurement situations, and fully exhausting the photon's "scattering potential" may introduce substantial errors.

3. Discussion

Unlike single-beam and multi-beam bathymetric systems, the coverage width of an airborne laser bathymetric system on the seabed is solely related to the UAV's flight altitude and is independent of the water depth being measured [40]. Moreover, a 100 m × 100 m sea surface reception field is unrealistic. The actual scanning point trajectory of the prototype system is illustrated in Figure 13.

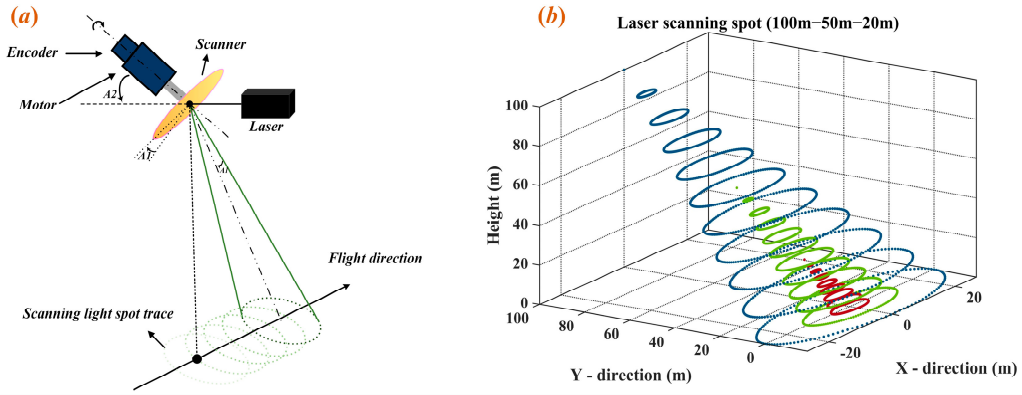

Figure 13. (**a**) Diagram illustrating the laser scanning approach. (**b**) Variation in sea surface coverage with changes in radar detection altitude.

When the airborne LiDAR was at different flight altitudes, the coverage of the scanning trajectory on the sea surface varied. The scanning trajectory of a single pass was elliptical, with the length of the major axis being approximately half the flight altitude of the drone. The maximum flight altitude of the drone carrying the active LiDAR was 100 m, and for the typical tests, underwater topography detection was conducted at 50 m. At this altitude, the sea surface area covered by the receiver's field of view in the marine LiDAR system encompasses the receiving plane of the selected simulation area. This ensures that, when using the Monte Carlo model to simulate the probability of echo photons returning to and being received at the sea surface, the detector size is appropriately represented. Although limited research has addressed this topic, our results and modeling efforts indirectly validate the suitability of the Monte Carlo random model for shallow marine environments, aligning well with the operational scope of marine LiDAR systems.

Since the raw signal actually received by the LiDAR contains all scattering events, while the LiDAR equation only accounts for single scattering and lacks a comprehensive formulation for multiple scattering, we can use simulated multiple scattering results to correct the raw signal. This indirect correction makes the simulation results more accurate.

To validate the reliability of the simulation results, a controlled experimental campaign was conducted. The test site measured 40 m in length and 11 m in width, and the survey was performed in a water tank containing six sample slots arranged in a 3 × 2 array. Each pair

of opposing slots contained the same bottom material type but with different thicknesses, differing by 10 cm. The three adjacent slots on one side were filled with gravel, sand, and rock, respectively. The tank was filled to a water depth of 50 cm, with low turbidity and a bottom slope ranging from 0° to 0.5°, resulting in a nearly flat underwater terrain.

An airborne LiDAR system was mounted on a linear track and scanned laterally across the tank to measure returns from the three different bottom types. The system parameters are detailed in Table 1. The high resolution and sensitivity of the LiDAR enabled the acquisition of accurate, full-waveform return data. As shown in Figure 14, the simulated results are used to correct the actual raw signal.

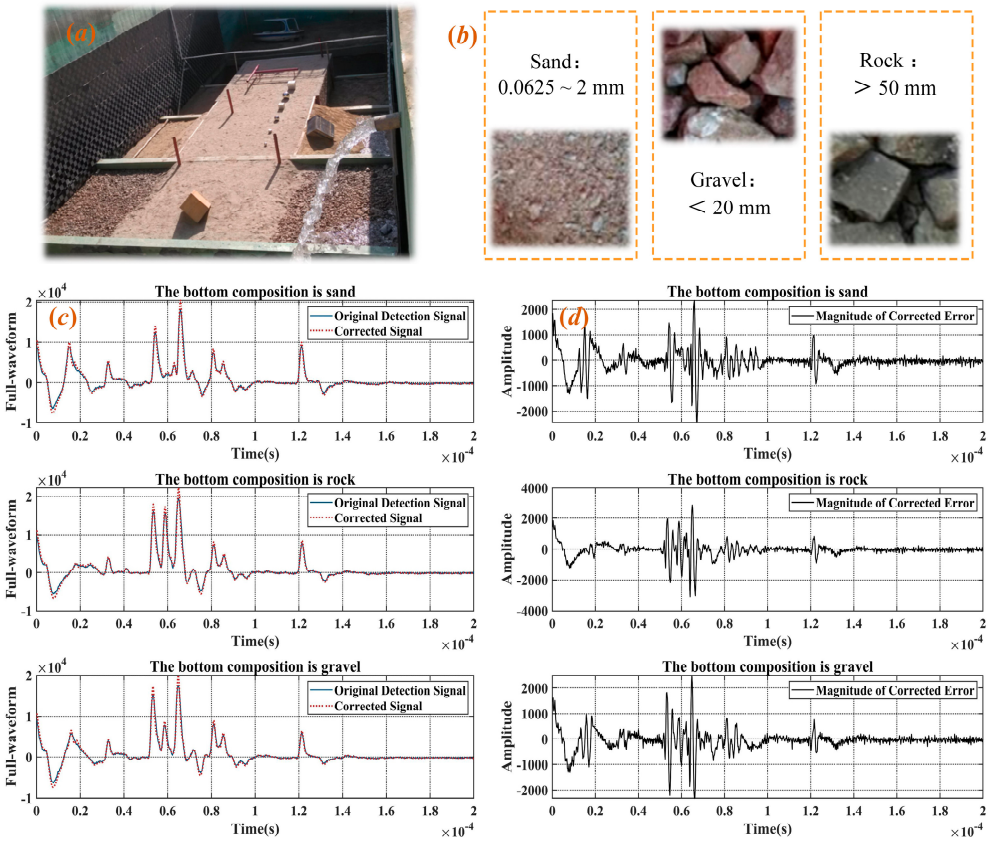

Figure 14. Correction of the raw signal using simulation results: (**a**) experimental setup; (**b**) selection of bottom material; (**c**) correction of the raw signal; (**d**) correction error.

When the water depth is relatively shallow, the simulation results show strong agreement with in-pool experimental measurements, as discussed above. This consistency validates the Monte Carlo model under the current experimental configuration and lends credibility to its application at greater depths. Accordingly, a representative depth range of 50–60 m is selected as the upper bound for further analysis, and the detection accuracy at this depth is corrected based on the model's predictions. Figure 15 illustrates the integration of the Monte Carlo random model with the laser transmission and reception methods used in the experimental system. As expressed in Equation (8), when considering laser transmission at depths greater than 50 m with more than three scatterings, the detection accuracy can be improved by 15.35~32.99% compared with the case where only a single scattering is considered. The simulation results can be applied to the current experimental systems to improve detection accuracy and efficiency.

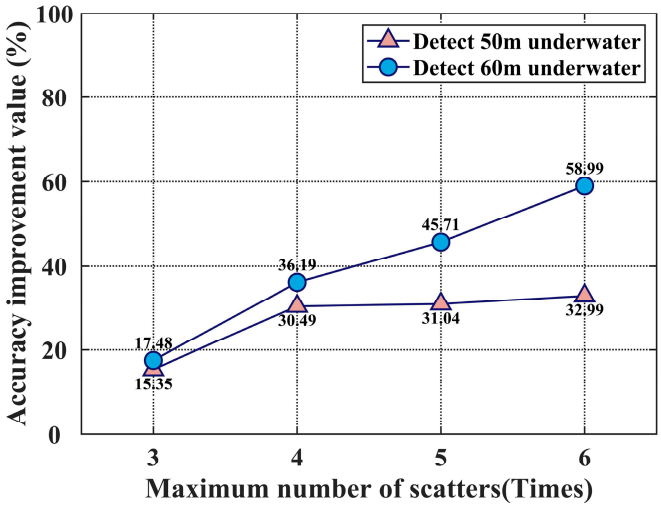

Figure 15. Comparison of accuracy improvement due to multiple scattering versus single scattering for underwater laser transmission at 50 and 60 m.

4. Conclusions

Based on the Beer–Lambert law and incorporating the parameters of typical Jerlov 1 clear coastal water, this model can quickly simulate the propagation of laser light in water and take into account multiple scattering events using the Monte Carlo method. By incorporating the laser-scanning methodology of the current experimental systems, this study emphasizes the impact of angle-induced changes in laser transmission on beam scattering. In practical applications, this translates to reconstructing the 3D structures of underwater targets by integrating the detection data with the laser incidence angle. The simulation results showed that accounting for three scattering events at a depth of 10 m reduced errors by at least 7% compared with considering only a single scattering event.

Subsequently, this study conducted a detailed analysis of pulse temporal broadening induced by scattering during laser transmission, using a combination of the Henyey–Greenstein phase function and the Monte Carlo model. The analysis focused on the comparative effects of three key parameters: transmission distance, asymmetry factor, and absorption coefficient. A novel approach is proposed to analyze the temporal broadening waveforms from a probabilistic perspective, offering a better explanation of the scattering and transmission processes during underwater laser propagation. A comparison with the actual test results confirmed the accuracy and validity of the simulation outcomes. Using this model, approximate laser transmission scenarios can be obtained by simply adjusting the underwater environmental parameters, thereby providing significant advantages in reducing experimental costs and time.

Finally, a Monte Carlo random model was employed to simulate the full round-trip process of photon transmission and reception, enabling analysis of the probability of echo signal detection by the LiDAR system. The model meticulously accounts for photon motion at the seabed boundary while filtering out photons that scatter to the detector immediately after laser entry. For depths exceeding 50 m, considering three or more scattering events instead of one can improve the detection accuracy by 15~33%. This improvement arises because photons undergoing more than three scattering events cannot return to the detector's field of view. For the current model, up to three scattering events provide sufficient correction for depths of 50 m or more. The proposed multiple-scattering simulation model shows strong agreement with the experimental prototype and yields results that can enhance detection accuracy and operational efficiency.

However, further training and the incorporation of additional parameters are necessary to better align the model with real-world measurement conditions. Furthermore, the

present study focuses on Jerlov I waters, which represent relatively idealized optical conditions. While this facilitates the simulation of deep-water light transport, real-world operations are subject to deviations due to various factors, including water type, sea state, and atmospheric conditions. Expanding the model to accommodate a broader spectrum of aquatic environments, therefore, represents a critical direction for future work, with the potential to enhance both its applicability.

Author Contributions: Conceptualization, R.D. and X.F.; methodology, X.M.; software, R.D.; validation, R.D., X.M. and X.F.; formal analysis, C.Y.; resources, X.M.; writing—original draft preparation, R.D.; writing—review and editing, T.L.; funding acquisition, C.Y. All authors have read and agreed to the published version of the manuscript.

Funding: This research was funded by the National Key Research and Development Program of China Grant 2022YFF0503703, B-type Strategic Priority Program of the Chinese Academy of Sciences Grant XDB0780000, and National Natural Science Foundation of China Grants 42130203 and 42394122.

Data Availability Statement: Data underlying the results presented in this paper are not publicly available at this time but may be obtained from the authors upon reasonable request.

Acknowledgments: We acknowledge the data resources from the College of Ocean Science and Engineering, Shandong University of Science and Technology.

Conflicts of Interest: The authors declare no conflicts of interest.

Abbreviations

The following abbreviations are used in this manuscript:

H-G	Heney-Greenstein phase function
LiDAR	Light Detection and Ranging
ALB	Airborne Laser Bathymetry

References

1. Irish, J.; White, T. Coastal engineering applications of high-resolution lidar bathymetry. *Coast. Eng.* **1998**, *35*, 47–71. [CrossRef]
2. Xu, P.; Liu, D.; Zhou, Y.; Liu, Q.; Bai, J.; Liu, Z.; Wu, L.; Shen, Y.; Liu, C. Modeling and analysis of oceanic lidar returns with multiple scattering. *J. Remote Sens.* **2020**, *24*, 142–148. [CrossRef]
3. Zhao, X.; Xia, H.; Zhao, J.; Zhou, F. Adaptive wavelet threshold denoising for bathymetric laser full-waveforms with weak bottom returns. *IEEE Geosci. Remote Sens. Lett.* **2022**, *19*, 1503505. [CrossRef]
4. Preisendorfer, R.W. *Radiative Transfer on Discrete Spaces*; Elsevier: Amsterdam, The Netherlands, 2014; Volume 74.
5. Arnush, D. Underwater light-beam propagation in the small-angle-scattering approximation. *J. Opt. Soc. Am.* **1972**, *62*, 1109–1111. [CrossRef]
6. Lutomirski, R.F.; White, M.B.; Stevenson, R. An analytic model for optical beam propagation through the marine boundary layer. In Proceedings of the Volume 0160, Ocean Optics V, 22nd Annual Technical Symposium, San Diego, CA, USA, 28–31 August 1978.
7. Ota, Y.; Higurashi, A.; Nakajima, T.; Yokota, T. Matrix formulations of radiative transfer including the polarization effect in a coupled atmosphere–ocean system. *J. Quant. Spectrosc. Radiat. Transf.* **2010**, *111*, 878–894. [CrossRef]
8. Mullen, L.; Contarino, V. Hybrid lidar-radar: Seeing through the scatter. *IEEE Microw. Mag.* **2002**, *1*, 42–48. [CrossRef]
9. Caflisch, R.E. Monte carlo and quasi-monte carlo methods. *Acta Numer.* **1998**, *7*, 1–49. [CrossRef]
10. Rubinstein, R.Y.; Kroese, D.P. *Simulation and the Monte Carlo Method*; John Wiley & Sons: Hoboken, NJ, USA, 2016.
11. Bucher, E.A. Computer simulation of light pulse propagation for communication through thick clouds. *Appl. Opt.* **1973**, *12*, 2391–2400. [CrossRef]
12. Bucher, E.A.; Lerner, R.M. Experiments on light pulse communication and propagation through atmospheric clouds. *Appl. Opt.* **1973**, *12*, 2401–2414. [CrossRef]
13. Lerner, R.M.; Summers, J.D. Monte Carlo description of time-and space-resolved multiple forward scatter in natural water. *Appl. Opt.* **1982**, *21*, 861–869. [CrossRef]
14. Chen, W.; Chen, P.; Zhang, H.; He, Y.; Tang, J.; Wu, S. Review of airborne oceanic lidar remote sensing. *Intell. Mar. Technol. Syst.* **2023**, *1*, 10.

15. Zhou, Y.; Chen, W.; Cui, X.; Malinka, A.; Liu, Q.; Han, B.; Wang, X.; Zhuo, W.; Che, H.; Song, Q.; et al. Validation of the analytical model of oceanic lidar returns: Comparisons with Monte Carlo simulations and experimental results. *Remote Sens.* **2019**, *11*, 1870. [CrossRef]
16. Iwabuchi, H. Efficient Monte Carlo methods for radiative transfer modeling. *J. Atmos. Sci.* **2006**, *63*, 2324–2339. [CrossRef]
17. Mullen, L.; Laux, A.; Cochenour, B. Propagation of modulated light in water: Implications for imaging and communications systems. *Appl. Opt.* **2009**, *48*, 2607–2612. [CrossRef]
18. Huang, Y.; He, Y.; Zhu, X.; Xu, G.; Zhang, C. Semi-analytical Monte Carlo simulation of underwater target echoes from a small UAV-based oceanic lidar. *Opt. Commun.* **2025**, *574*, 131157. [CrossRef]
19. Zhang, J.; Kou, L.; Yang, Y.; He, F.; Duan, Z. Monte-Carlo-based optical wireless underwater channel modeling with oceanic turbulence. *Opt. Commun.* **2020**, *475*, 126214. [CrossRef]
20. Li, W.; Du, L.; Meng, X.; Liu, J.; Li, Y.; Zhang, X.; Wan, D. Adaptive Denoising for Airborne LiDAR Bathymetric Full-Waveforms Using EMD-Based Multi-Resolution Analysis. *IEEE Geosci. Remote Sens. Lett.* **2024**, *21*, 6500705.
21. Jerlov, N.G. *Marine Optics*; Elsevier: Amsterdam, The Netherlands, 1976; Volume 14.
22. Liou, K.-N. *An Introduction to Atmospheric Radiation*; Elsevier: Amsterdam, The Netherlands, 2002; Volume 84.
23. Mobley, C.D. *Light and Water: Radiative Transfer in Natural Waters*; Academic Press: Cambridge, MA, USA, 1994.
24. Gordon, H.R. *Physical Principles of Ocean Color Remote Sensing*; University of Miami: Coral Gables, FL, USA, 2019.
25. Du, L.; Wan, D.; Meng, X.; Li, W.; Liang, G.; Li, H. Classification of underwater sediments in lab based on LiDAR full-waveform data. *J. Mar. Sci. Eng.* **2025**, *13*, 624. [CrossRef]
26. Liu, Y.; Guo, K.; He, X.; Xu, W.; Feng, Y. Research progress of airborne laser bathymetry technology. *Geomat. Inf. Sci. Wuhan Univ.* **2017**, *42*, 1185–1194.
27. Liang, J.; Yang, K.; Xia, M.; Zhang, X.; Lei, X.; Zheng, Y.; Tan, D. Monte Carlo simulation for modulated pulse bathymetric light detecting and ranging systems. *J. Opt. A Pure Appl. Opt.* **2006**, *8*, 415. [CrossRef]
28. Zege, E.P.; Katsev, I.L.; Prikhach, A.S.; Ludbrook, G.D.; Bruscaglioni, P. Analytical and computer modeling of oceanic lidar performance. In Proceedings of the 12th International Workshop on Lidar Multiple Scattering Experiments, Oberpfaffenhofen, Germany, 10–12 September 2002; Volume 5059.
29. Zege, E.P.; Katsev, I.L.; Prikhach, A.S.; DeWeert, M.J.; Saito, T.T.; Guthmuller, H.L. Recent advancement in computer simulating performance of the sounding and detecting ocean lidars in very shallow waters. In Proceedings of the Volume 6204, Photonics for Port and Harbor Security II, Florida, Orlando, FL, USA, 18–20 April 2006; Volume 6204.
30. Nan, A.; Wu, W.; Kan, W. Implementation and Optimization of Function Expansion Tallies Based on Track Length Estimation Method in RMC. *Nucl. Power Eng.* **2024**, *45*, 78–84.
31. Buras, R.; Mayer, B. Efficient unbiased variance reduction techniques for Monte Carlo simulations of radiative transfer in cloudy atmospheres: The solution. *J. Quant. Spectrosc. Radiat. Transf.* **2011**, *112*, 434–447. [CrossRef]
32. Li, Z.; Wang, L.; Du, L.; Meng, X. Research on Airborne LiDAR Bathymetry and Data Processing Algorithms. In Proceedings of the 2023 5th International Conference on Artificial Intelligence and Computer Applications (ICAICA), Dalian, China, 28–30 November 2023.
33. Leathers, R.A.; Downes, T.V.; Davis, C.O.; Mobley, C.D. Monte Carlo radiative transfer simulations for ocean optics: A practical guide. *Memo. Rep. A* **2004**, 426624.
34. Wang, C.-K.; Philpot, W.D. Using airborne bathymetric lidar to detect bottom type variation in shallow waters. *Remote Sens. Environ.* **2007**, *106*, 123–135. [CrossRef]
35. Liu, X.; Tulldahl, H.M.; Axelsson, A. An overview of the airborne bathymetric lidar reflectance data processing. In Proceedings of the International Symposium on Lidar and Radar Mapping 2011: Technologies and Applications, Nanjing, China, 26–29 May 2011; Volume 8286.
36. Yang, F.; Qi, C.; Su, D.; Ma, Y.; He, Y.; Wang, X.H.; Liu, J. Modeling and analyzing water column forward scattering effect on airborne LiDAR bathymetry. *IEEE J. Ocean. Eng.* **2023**, *48*, 1373–1388. [CrossRef]
37. Yingluo, Z.; Yingmin, W.; Aiping, H. Analysis of underwater laser transmission characteristics under Monte Carlo simulation. In Proceedings of the 2018 OCEANS-MTS/IEEE Kobe Techno-Oceans (OTO), Kobe, Japan, 28–31 May 2018.
38. Morel, A.; Maritorena, S. Bio-optical properties of oceanic waters: A reappraisal. *J. Geophys. Res. Ocean.* **2001**, *106*, 7163–7180. [CrossRef]
39. Zaneveld, J.R.V. Light and water: Radiative transfer in natural waters. *Bull. Am. Meteorol. Soc.* **1995**, *76*, 60–63.
40. Costa, B.; Battista, T.; Pittman, S. Comparative evaluation of airborne LiDAR and ship-based multibeam SoNAR bathymetry and intensity for mapping coral reef ecosystems. *Remote Sens. Environ.* **2009**, *113*, 1082–1100. [CrossRef]